PAPER

PAMAM G4.5-chlorin e6 dendrimeric nanoparticles for enhanced photodynamic effects†

Estelle Bastien,[a,b,c] Raphaël Schneider,[d] Steffen Hackbarth,[e] Dominique Dumas,[f] Jordane Jasniewski,[g] Beate Röder,[e] Lina Bezdetnaya[a,b,c] and Henri-Pierre Lassalle*[a,b,c]

There is currently great interest in the development of efficient and specific carrier delivery platforms for systemic photodynamic therapy. Therefore, we aimed to develop covalent conjugates between the photosensitizer chlorin e6 (Ce6) and PAMAM G4.5 dendrimers. Singlet oxygen generation (SOG) efficiency and fluorescence emission were moderately affected by the covalent binding of the Ce6 to the dendrimer. Compared to free Ce6, PAMAM anchored Ce6 displays a much higher photodynamic effect, which is ascribable to better internalization in a tumor cell model. Intracellular fate and internalization pathway of our different compounds were investigated using specific inhibition conditions and confocal fluorescence microscopy. Free Ce6 was shown to enter the cells by a simple diffusion mechanism, while G4.5-Ce6-PEG internalization was dependent on the caveolae pathway, whereas G4.5-Ce6 was subjected to the clathrin-mediated endocytosis pathway. Subcellular localization of PAMAM anchored Ce6, PEGylated or not, was very similar suggesting that the nanoparticles behave similarly in the cells. As a conclusion, we have demonstrated that PEGylated G4.5 PAMAM-Ce6 dendrimers may offer effective biocompatible nanoparticles for improved photodynamic treatment in a preclinical tumor model.

[a]*Université de Lorraine, Centre de Recherche en Automatique de Nancy, Campus Sciences, Vandœuvre-lès-Nancy, France. E-mail: h.lassalle@nancy.unicancer.fr*
[b]*Centre National de la Recherche Scientifique, Centre de Recherche en Automatique de Nancy, France*
[c]*Research Department, Institut de Cancérologie de Lorraine, Avenue de Bourgogne, 54519 Vandœuvre-lès-Nancy, France*
[d]*Université de Lorraine, Laboratoire Réactions et Génie des Procédés (LRGP), UMR 7274, CNRS, 1 rue Grandville, BP 20451, 54001 Nancy Cedex, France*
[e]*Institut für Physik, Humboldt, Universität zu Berlin, Newtonstrasse, Berlin, Germany*
[f]*Université de Lorraine, Plateforme IBISA d'Imagerie et de Biophysique Cellulaire de Nancy, IMOPA7365, FR3209 BMCT, Centre National de la Recherche Scientifique, Vandœuvre-lès-Nancy, France*
[g]*Université de Lorraine, Laboratoire d'ingénierie des biomolécues (LIBio), 2 avenue de la Forêt de Haye, Vandœuvre-lès-Nancy, France*
†Electronic supplementary information (ESI) available. See DOI: 10.1039/c5pp00274e

Introduction

Photodynamic therapy (PDT) is a minimally-invasive photochemical-based approach that uses a combination of a light-activated drug (photosensitizer, PS) and the light of a specific wavelength to damage the target tumor tissue by generating reactive oxygen species.[1] Among them, molecular oxygen in its first excited electronic state, so called singlet oxygen ($^1O_2$), is commonly agreed to be the cytotoxic key agent in photo-dynamic action. PDT has a clinical reality since several photosensitizers have obtained approval for the treatment of localized and light-accessible tumors.

For safe and effective therapy with limited side effects, a PS should reach targeted cells at a certain concentration threshold together with a low accumulation in healthy cells. However, to achieve this goal, two major problems are often encountered. Firstly, most PS molecules are hydrophobic and aggregate easily in aqueous media, resulting in reduced singlet oxygen generation[1] and difficulties with intravenous delivery.[2] Secondly, PSs generally display a low or moderate selectivity to cancer cells, thus requiring high PS concentrations in clinical protocols, yielding serious adverse effects. To overcome these drawbacks, the use of vectors for PS tumor targeting was suggested, providing an improvement in PS solubility, protecting from PS deactivation reactions and favoring tumor targeting through the enhanced permeability and retention (EPR) effect. EPR is inherent to many solid tumors due to leaky vasculature and poor lymphatic drainage.[3] Currently basic research in PDT focuses mainly on the development of carrier systems for targeting tumor tissue.[4] With this aim, biocompatible nanocarriers for PS delivery such as lipid-based nanoparticles (NP),[5,6] polymer-based NPs,[7,8] micelles[9,10] or silica-based NPs,[11] have been designed. Dendrimers have been proposed as building blocks for PDT drug delivery systems already in 2001.[12] Dendrimers are regular hyperbranched macro-

molecules of a few nanometers in size (2–10 nm) with many functional groups at their surface which allow anchoring therapeutic molecules such as photosensitizers, stealth elements (polyethylene glycol), or targeting moieties on their surface, while controlling the size and lipophilicity of the carrier. Given their low cytotoxicity and their water solubility many types of poly(amido amine) (PAMAM) dendrimers appear as a very attractive class of biocompatible nanovectors for drug targeting in cells and tissues.[13–15]

So far, three different assemblies of dendrimer-based carrier systems have been reported in the field of PDT. The first uses a porphyrin or phthalocyanine as the starting core with a dendron grafted on each pyrrole unit. The Kataoka group reported good photodynamic efficacy of these NPs excitable in the far red, making them eligible for *in vivo* applications.[16,17] The second construction consists of photosensitizers like protoporphyrin IX (PpIX) encapsulated in the dendrimer, which can be progressively released into the medium.[18] The last class of structures is based on the covalent binding of PS on the periphery groups of dendrimers. As we recently demonstrated that PpIX prodrug, ALA (5-aminolaevulinic acid) can be attached to dendrimers *via* a cleavable ester bond, resulting in a higher synthesis rate and better tumor selectivity of PpIX *in vivo* compared with free ALA.[19] Hackbarth *et al.*[12] achieved an average loading of 12–13 molecules of pheophorbide a (Pheo) to one diaminobutane (DAB) dendrimer molecule with 16 available binding sites. However, singlet oxygen generation of covalently linked dye molecules was dramatically reduced compared with free Pheo, mostly due to trap formation (excitonic interaction of at least two neighboring chromophores) combined with Förster-energy transfer between different Pheo molecules at the surface of highly loaded dendrimers. Strong quenching effects were also reported for high loaded peryleneimide–terrylenediimide polyphenyl dendrimers.[12,20]

The present paper evaluates the therapeutic *in vitro* efficiency of the photoactive NP consisting of the PS chlorin e6 (Ce6) covalently bound to a biocompatible PAMAM G4.5 dendrimer. To avoid strong quenching effects, only 25% of the carboxylic acid groups present at the dendrimer surface were modified with the PS. Herein, we describe the photophysical properties, subcellular localization and internalization pathway of Ce6-grafted dendrimers (G4.5-Ce6). Changes observed in cellular uptake and phototoxicity upon PEGylation of the NPs were also evaluated.

Experimental

Materials and general procedure

Starbust polyamidoamine (PAMAM) dendrimer generation 4.5 (5 wt% in methanol, containing 128 surface carboxylate groups, MW 26 228 g mol^{-1}), benzotriazole-1-yl-oxy-tris-(dimethylamino)phosphonium hexafluorophosphate (BOP), poly-(ethylene glycol) methyl ether (MW 2000 g mol^{-1}), dicyclohexylcarbodiimide (DCC), 4-dimethylaminopyridine (DMAP),
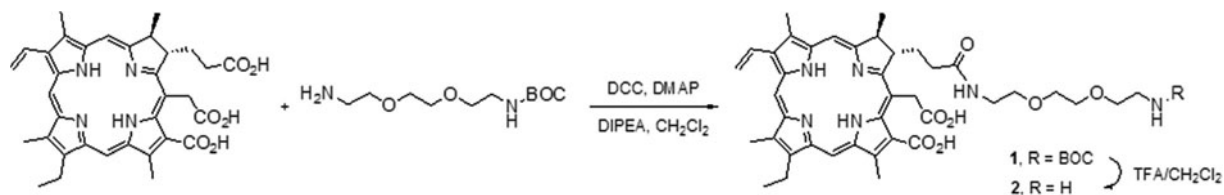
N-hydroxysuccinimide (NHS), diisopropylethylamine (DIPEA), 2,2′-(ethylenedioxy)bis(ethylamine), trifluoroacetic acid (TFA), chlorpromazine, genistein, 5-(*N*-ethyl-*N*-isopropyl)amiloride (EIPA), DMSO, MeOH and dichloromethane were purchased from Sigma-Aldrich (St Louis, MO, USA). Chlorin e6 (Ce6) was purchased from Livchem (Frankfurt, Germany). RPMI 1640 medium, L-glutamine, foetal bovine serum, penicillin–streptomycin and phosphate-buffered saline (PBS) were supplied by GibcoBRL (Merelbeke, Belgium). Ultrapure water was used through all the experiments. All starting materials and organic solvents were directly used without further purification. *N*-Boc-protected 2,2′-(ethylenedioxy)bis(ethylamine) was prepared according to Trester-Zedlitz.[21]

Synthesis of chlorin e6 – PAMAM dendrimer nanoparticles.

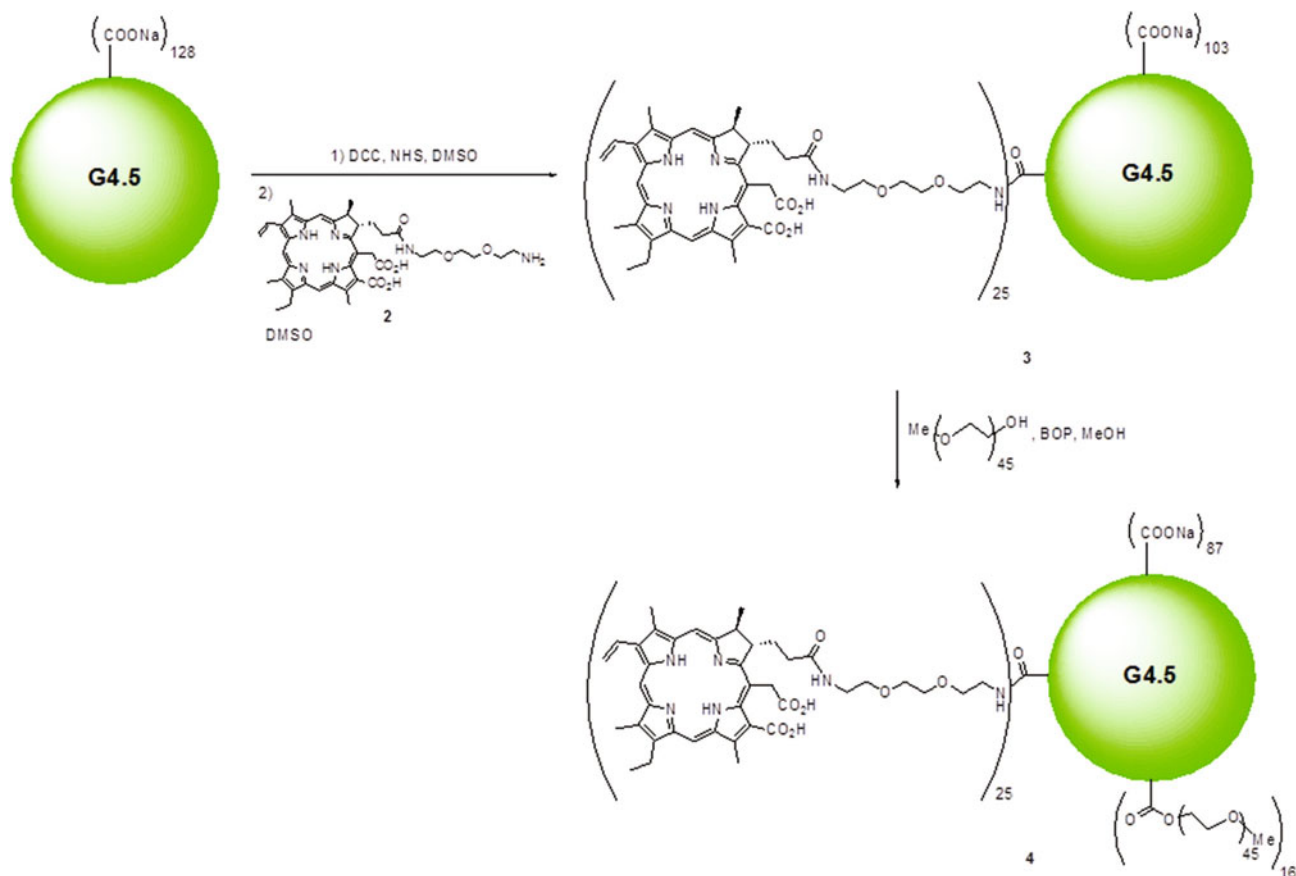**Coupling of Ce6 with *N*-Boc-protected 2,2′-(ethylenedioxy)bis-(ethylamine).** Under an argon atmosphere in the dark, Ce6 (100 mg, 1.677 × 10^{-4} mol) was dissolved in 58 mL of anhydrous CH$_2$Cl$_2$. DCC (34.6 mg, 1.677 × 10^{-4} mol) and DMAP (4 mg, 3.27 × 10^{-5} mol) were added to the Ce6 solution and the mixture was stirred for 10 min at room temperature. Separately, *N*-Boc-protected 2,2′-(ethylenedioxy)bis(ethylamine) (50 mg, 2.012 × 10^{-4} mol) and DIPEA (26 mg, 2.012 × 10^{-4} mol) were dissolved in 10 mL CH$_2$Cl$_2$. This solution was added to the activated Ce6 and the mixture was stirred at room temperature for 10 h. The progress of the reaction was monitored by thin layer chromatography using MeOH/CH$_2$Cl$_2$ (10 : 90) as the eluent. The precipitant dicyclohexylurea was removed by filtration through a glass filter. The reaction mixture was then poured into a separation funnel, washed with water (25 mL) and saturated brine (25 mL), dried over Na$_2$SO$_4$ and the solvent evaporated under reduced pressure. Compound **1** (Scheme 1) was isolated in 82% yield after column chromatography on silica gel using MeOH/CH$_2$Cl$_2$ (10 : 90) as the eluent.

Deprotection of the BOC group. Synthesis of compound 2. In the dark under an argon atmosphere, compound **1** (100 mg, 1.187 × 10^{-4} mol) was treated with TFA/CH$_2$Cl$_2$ (1 : 1, 7 mL) at room temperature. After being stirred for 2 h, TFA and CH$_2$Cl$_2$ were evaporated. The residue was taken up in CH$_2$Cl$_2$ (30 mL) and stirred with K$_2$CO$_3$. After filtration, the organic layer was concentrated under reduced pressure and compound **2** was obtained in 96% yield. Chlorin **2** (Scheme 1) was used without further purification for the next step.

Anchorage of 2 at the surface of G4.5 PAMAM dendrimer. The anchorage of **2** at the surface of the G4.5 PAMAM dendrimer (Scheme 2) was conducted according to a synthetic procedure described by Hargus *et al.* with slight modifications.[22] Briefly, methanol was first evaporated *in vacuo* from the commercial G4.5 PAMAM dendrimer solution. The obtained oil (235 mg, 8.95 × 10^{-6} mol) was solubilized in anhydrous DMSO (10 mL). DCC (118.2 mg, 5.73 × 10^{-4} mol) and NHS (98.91 mg, 8.585 × 10^{-4} mol) were then added to activate surface carboxylate functions and the solution was stirred for 15 h at room temperature under an argon atmosphere. Chlorin **2** (0.187 mg, 2.57 × 10^{-4} mol) in 10 mL DMSO was then added and the mixture was stirred for 24 h. The precipitant dicyclohexylurea

2204 | *Photochem. Photobiol. Sci.*, 2015, **14**, 2203–2212

This journal is © The Royal Society of Chemistry and Owner Societies 2015

Scheme 1 Synthetic route for the preparation of diamino PEG-functionalized chlorin **2**.

Scheme 2 Synthetic route to multifunctional PAMAM dendritic NPs **3** and **4**.

was removed by filtration through a glass filter. The reaction medium was then diluted with water (50 mL) and dialyzed using a dialysis bag (molecular weight of 6–8000 Da cut off) against ultrapure water for 72 h, the water being changed every 24 h, to remove low MW contaminants and unreacted **2**. The solution was finally lyophilized to provide pure **3** in 91% yield. Attachment of **2** to the dendrimer provided exclusively compound **3**, requiring only dialysis for the workup, thus facilitating scale up (Scheme 2).

Surface PEGylation of 3

Finally, in order to increase the blood circulation times and the accumulation in tumor tissue, poly(ethylene glycol) methyl ether (mPEG$_{2000}$-OMe, MW 2000) was used to cover *ca.* 8% of

the carboxylic groups on the surface of the periphery of dendrimer **3** (Scheme 2).

Surface PEGylation of **3** was achieved by formation of ester bonds between surface carboxylate groups of the dendrimer and poly(ethylene glycol) methyl ether (MW 2000, mPEG$_{2000}$-OMe) using BOP as a coupling agent and methanol as a solvent.[23] Under argon and in the dark, compound **3** (0.180 g, 4.08×10^{-6} mol) and BOP (0.086 g, 1.95×10^{-4} mol) were dissolved in 20 mL anhydrous methanol. mPEG$_{2000}$-OMe (0.130 g, 6.537×10^{-5} mol) was then added and the mixture was stirred for 3 days at room temperature. Methanol was next evaporated *in vacuo*. The residue was solubilized in water (30 mL) and dialyzed using a dialysis bag (molecular weight 6–8000 cut off) against ultrapure water for 48 h, the water being changed every

This journal is © The Royal Society of Chemistry and Owner Societies 2015

Photochem. Photobiol. Sci., 2015, **14**, 2203–2212 | **2205**

24 h, to remove low MW contaminants and unreacted mPEG$_{2000}$-OMe without significant lowering of the yield of the PEGylated dendrimer. The solution was finally lyophilized to provide compound **4**.

Characterization

The Ce6 concentration of G4.5-Ce6 (±PEG) solution was determined by UV/Vis spectroscopy (Lambda 35 UV/Vis spectrofluorimeter LS55 Perkin-Elmer). Free Ce6 was dissolved in ethanol at different concentrations to generate a standard curve and calculate the molar extinction coefficient at 665 nm. The amount of the Ce6 content in PAMAM G4.5 solution was calculated assuming the same extinction coefficient as for Ce6 in solution. Fluorescence spectra of free Ce6 and G4.5-Ce6 (±PEG) were recorded using an LS55 fluorescence spectrometer (Perkin-Elmer). All measurements were done in ethanol at the dye concentration of 0.5 μg mL^{-1}; at this dye concentration the optical density did not exceed 0.1 at λ_{exc} = 410 nm. The hydrodynamic diameter and the zeta potential of G4.5-Ce6 and G4.5-Ce6-PEG NP were determined using a Malvern Zetasizer Nano ZS (173°, 532 nm, 25 °C). The samples were prepared at a concentration of 1 μg mL^{-1} in MilliQ water and filtered at 0.1 μm. The hydrodynamic diameter is reported as the volume-weighted average of twelve measurements.

For zeta potentials a voltage of 100 V was applied at 25 °C. The samples were loaded into pre-rinsed folded capillary cells; at least three independent measurements were made.

Evaluation of the singlet oxygen generation (SOG)

Singlet oxygen luminescence kinetics have been recorded using time correlated multi photon counting employing the NIR PMT H10330-45 from Hamamatsu as a detector. The setup is identical to the $^1O_2$ luminescence detection system TCMPC1270 of SHB Analytics, Germany. The excitation intensity profile, temporal shape and spectrum of the pulsed LED excitation around 400 nm are described by Hackbarth *et al.*[24] The optical density of the samples and reference is adjusted to 0.1 at 400 nm. Singlet oxygen quantum yield of the reference substance (5,10,15,20-tetrakis(*N*-methyl-4-pyridyl)-21H,23H-porphine, TMPyP) was previously measured to be 0.70 ± 0.05 in ethanol. This value is consistent with the value reported earlier by Wilkinson *et al.*[25]

Cell culture

Human pharynx squamous cell carcinoma (FaDu) cell line was obtained from the American Type Culture Collection (ATCC® HTB-43™). FaDu cells were grown in humidified incubator at 37 °C, 5% CO$_2$, in RPMI 1640 medium (Roswell Park Memorial Institute) supplemented with 10% fetal bovine serum (FBS), 1% penicillin–streptomycin and 1% L-glutamine.

In vitro photocytotoxicity assessed by clonogenic assay

Cells were seeded into 6-wells plates at a concentration of 9 × 10^4 cells per well. Following incubation for 48 h, the cells were washed with PBS and incubated for 24 h in RPMI supplemented with 2% FBS and containing each compound at

varying concentrations. Stock solution of Ce6 was prepared in DMSO so that the concentration of solvent never exceeded 0.1% in the medium. G4.5-Ce6 (±PEG) was prepared in water. After two consecutive washings with PBS, fresh medium was added and cells were irradiated at 652 nm with a Ceralas PDT diode laser (CeramOptec GmbH, Bonn, Germany) at a fluence of 2.5 J cm^{-2} with a fluence rate of 10 mW cm^{-2}. The cell viability was then evaluated by a clonogenic assay. The cells were washed and incubated with trypsin-EDTA to prepare single-cell suspensions from monolayer cultures. Viable cells were then seeded in a 6-well plate at a concentration of 500 cells per well. Ten days later, the culture medium was removed and cells were washed and incubated 5 min at room temperature successively with 70% ethanol and 1% crystal violet solution. Then the colonies were washed and counted. Results are given as the percentage of surviving cells normalized to those obtained from the control groups (drug, no light). To determine the dark toxicity of the compounds, well plates were prepared in the same manner as described above without irradiation.

Cellular uptake assay

FaDu cells (3 × 10^4 cells per well) were seeded in 24-well plates, 48 h later the cells were washed with PBS and incubated for 24 h in RPMI supplemented with 2% FBS and containing each compound under investigation at varying concentrations. After three consecutive washings with PBS, Solvable™ (Perkin-Elmer) was added for 2 h at 50 °C for solubilizing cells. The cellular uptake of Ce6 was determined from fluorescence calibration curves constructed by plotting the peak height of Ce6 standard solutions in Solvable™. The calibration was linear within this range. Error bars are the standard deviation for three independent experiments.

Internalization pathway inhibition studies

FaDu cells (3 × 10^4 cells per well) were seeded in 24-well plates, and incubated for 48 h prior to the addition of NPs. Then, the cells were pre-incubated in RPMI 2% FBS for 30 min with either 10 μg ml^{-1} chlorpromazine (inhibitor of clathrin-dependent endocytosis), 400 μM genistein (inhibitor of caveolae-dependent endocytosis) or 100 μM EIPA (inhibitor of macropinocytosis). The impact of low temperature was studied by pre-incubating cells at 4 °C for 30 min prior to exposure to the compounds. After this pre-incubation, G4.5-Ce6 (±PEG) (final concentration 0.5 μg ml^{-1}) were added and incubated for 60 min, either in the presence of the inhibitors or at 4 °C. Ce6 uptake was measured as previously described. Results are given as the percentage of uptake normalized to those obtained from control groups (without inhibitors or at 37 °C).

Subcellular localization of NP with or without PEG

FaDu cells (1 × 10^4 cells per ml) were plated into four well chambers Slideflask (Nunc, Roskilde, Denmark), incubated in the dark at 37 °C with 2 μg ml^{-1} of free Ce6 or NP-Ce6 (±PEG) during 24 h, then rinsed and incubated with organelle specific fluorescent probes. The ER was labelled with DiOC$_6$ dye, applied for 1 min at a final concentration of 2.5 mg ml^{-1}. To

2206 | *Photochem. Photobiol. Sci.*, 2015, **14**, 2203–2212

This journal is © The Royal Society of Chemistry and Owner Societies 2015

identify the Golgi apparatus, the cells were labelled with 5×10^6 M of NBD-C_6 ceramide for 30 min at 4 °C, then rinsed with cold PBS solution and re-incubated in the RPMI 9% FBS at 37 °C for the next 30 min. The staining of mitochondria and lysosome was performed by cell incubation with 2×10^{-7} M of MitoTracker® Green or 7.5×10^{-8} M of LysoTracker® Green for 30 min at 37 °C. Before observation, the cells were washed with PBS to remove dyes. Double-stained cells were observed with a confocal laser-scanning microscope (Leica SP5 X AOBS LCSM; Leica microsystem, Wetzlar, Germany). A white light laser (SuperK, extreme supercontinuum lasers, NKT Photonics) was used to excite organelle specific fluorescent probes and Ce6 at appropriate wavelengths. Fluorescence emission of Ce6 (peak 665 nm) was collected from 645 to 690 nm on one channel (red), and fluorescence from organelle specific labelling was collected from 505 to 550 nm on a second channel (green), with the pinhole locked at 600 μm. A water immersion objective (×63) was used to capture each image of 1024 × 1024 pixels. No visible photobleaching was observed during image acquisition. Colocalization was quantified with the Pearson's correlation coefficient (PCC). The absolute PCC values of 1–0.7 indicate a relatively strong correlation, 0.69–0.36 indicate a moderate correlation, 0.35–0.2 indicate a weak correlation, and <0.2 indicates the absence of a correlation.[26,27] The square of the PCC value represents the percentage of Ce6 fluorescence signal arising from the fluorescence of the organelle marker.[26]

Fluorescence-lifetime imaging

The cell images were observed with a CLSM (FluoView™ FV1000, Olympus) with FLIM-extension (Pico Quant, Berlin). Fluorophores were excited with a nanosecond pulse laser at λ_{ex} = 440 nm. FaDu cells were incubated 24 h with G4.5-Ce6 (±PEG) or free Ce6. After two consecutive washings with PBS, fresh medium was added and cells were analyzed by using the FLIM equipment before and after irradiation (white light 10 mW cm^{-2}; 5 min).

Statistical analysis

Statistical significance among two conditions was assessed using the nonparametric Mann–Whitney test. P-value was considered at the 5% level of significance to deduce inference of the significance of the data.

Results and discussion

Physical and photophysical characterization

The hydrodynamic diameter determined by DLS (Table 1) is 6.3 nm for G4.5-Ce6 and 12 nm for G4.5-Ce6-PEG (PDI of 0.23 and 0.33, respectively). The surface charge exhibits a negative zeta potential of −17.7 mV and −8.9 mV for G4.5-Ce6 and G4.5-Ce6-PEG, respectively, due to the presence of the carboxylate functions at neutral pH.

Absorption and fluorescence spectra of free Ce6, G4.5-Ce6 and G4.5-Ce6-PEG are shown in Fig. 1. The covalent binding between Ce6 and the dendrimer results in slight changes in the absorption spectra. A small bathochromic shift of the lowest Q-band (2 nm) together with a moderate increase of the bandwidth of all the absorption bands are observed for the G4.5-Ce6 and G4.5-Ce6-PEG compared to free Ce6 (Table 1, Fig. 1A). Similar effects were previously observed for comparable nanohybrids[12] and have been attributed to local changes of the refractive index due to the vicinity of the PS to each other.[28] This also indicates that the attached Ce6 molecules interact partly, without general aggregation or structural modification when Ce6 was loaded with amide bonds on the PAMAM G4.5 dendrimers.

The fluorescence spectra of the NPs are very similar to Ce6 in ethanol solution (Fig. 1B), but the fluorescence quantum yield Φ_F is reduced after covalent binding (0.11 and 0.09 for G4.5-Ce6 and G4.5-Ce6-PEG, respectively) compared to free Ce6 (0.16)[29] (Table 1). The singlet oxygen quantum yield Φ_Δ is reduced to 0.31 and 0.26, for G4.5-Ce6 and G4.5-Ce6-PEG, respectively compared to free Ce6 (0.55). The statistical loading of Ce6 on the dendrimer results in different PS–PS distances. Few of them are close enough for an excitonic interaction, resulting in non-radiative deactivation of the excited singlet state. However, the majority of Ce6 molecules at the same dendrimer are obviously sufficiently isolated to avoid Forster transfer towards this PS pair. Therefore the probability of quenching is much lower compared to the dendrimer constructs reported in Hackbarth et al.[12] The Förster radius of Ce6 can be calculated as 23 Å, while the average distance between PSs at one dendrimer is 22 Å, when computed from the measured diameter of our G4.5-Ce6 dendrimer (6.3 nm, Table 1) and the average number of Ce6 molecules linked on the dendrimer.[32] Due to the strong dependency of the distance

Table 1 Photophysical properties

Photosensitizer system	λ_{max} (nm) (Q-absorption)	λ_{max} (nm) (fluorescence)	Φ_{FL} (±0.05) (fluorescence)	Φ_Δ (±0.02) (singlet oxygen)	Hydrodynamic diameter (nm)/PDI	Zeta potential (mV)
Ce6	662.5	669	0.16	0.55	N.A.	N.A.
G4.5-Ce6	665	670.5	0.11	0.26	6.3/0.23	−17.7
G4.5-Ce6-PEG	664.5	671.5	0.09	0.31	12/0.33	−8.9

λ_{max}: maximal wavelength of absorption and fluorescence (excitation wavelength: 410 nm) in the last Q-band of the visible spectrum in ethanol. Φ_Δ: singlet oxygen quantum yield. Φ_{FL}: fluorescence quantum yield. Since the fluorescence quantum yield and singlet oxygen quantum yield are determined by comparison with a known reference, the error is mainly caused by the error of the reference, and thus it has the same percentage for all samples.
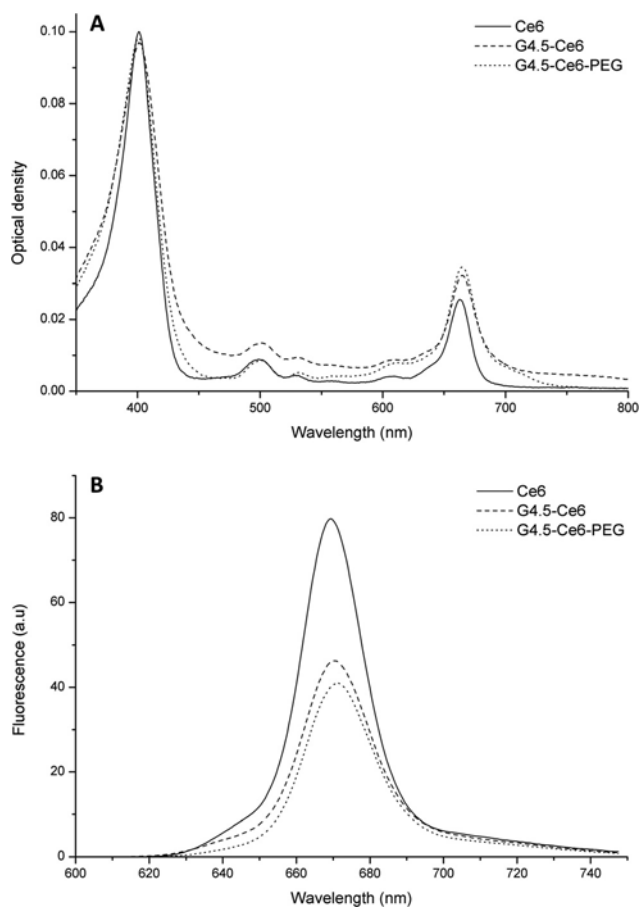
This journal is © The Royal Society of Chemistry and Owner Societies 2015

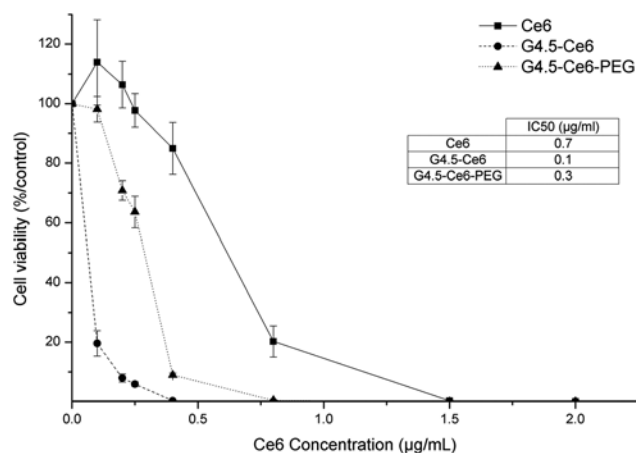*Photochem. Photobiol. Sci.*, 2015, **14**, 2203–2212 | **2207**

Fig. 2 *In vitro* antitumor activity of free Ce6 (square), G4.5-Ce6 (round) and G4.5-Ce6-PEG (triangle) after photoirradiation (2.5 J cm^{-2}). FaDu cells were treated 24 h with various concentrations of free Ce6 or vectorized with G4.5 dendrimers (±PEG). IC$_{50}$: concentration of the PS inducing 50% of cell death.

Fig. 1 Absorption (A) and fluorescence emission (B) spectra of Ce6 (solid line), G4.5-Ce6 (dashed line) and G4.5-Ce6-PEG (dot line) in ethanol. Ce6 concentration adapted to reach an OD of 0.1 in the Soret band.

between molecules on the FRET (factor of 10^6), variation in the distance of only 20% causes the molecule to behave like a monomer in solution or undergo nearly exclusively FRET resulting in quenching. Quenching of around 40%–50% (Table 1) appears to be reasonable in this context.

Photodynamic activity and cellular uptake

The viability of FaDu cells was evaluated by using the clonogenic assay as a function of PS concentration. No dark cytotoxicity was observed after treatment with Ce6, G4.5-Ce6 or G4.5-Ce6-PEG in the range of the tested concentrations (Fig. S1†). However, when irradiated, both dendrimer based NPs showed a remarkable and concentration dependent phototoxicity (Fig. 2). The IC$_{50}$ values, defined as the concentration of PS at which 50% of tumor cells survive after photoirradiation, are displayed in the inset of Fig. 2. The IC$_{50}$ of free Ce6 after 24 h incubation and irradiation (2.5 J cm^{-2}) is 0.7 μg ml^{-1} (Fig. 2). This value is consistent with other studies using Ce6 under similar irradiation conditions.[30,31] The IC$_{50}$ of G4.5-Ce6 and G4.5-Ce6-PEG dendrimers were respectively 3 and 7 times lower (0.1 μg ml^{-1} and 0.3 μg ml^{-1}) (Fig. 2). The same order of

IC$_{50}$ was reported earlier for aryl ether dendrimer Zn–porphyrin complexes under similar experimental conditions.[32]

Ce6 cellular uptake was significantly enhanced once anchored at the surface of the dendrimer compared to free PS (Fig. 3). Independent of the incubation concentration, the mean uptake (slope of the uptake fitting line) is increased by a factor of 10 for G4.5-Ce6-PEG and a factor of 22 for G4.5-Ce6 compared to free Ce6. The G4.5-Ce6 demonstrated two-fold higher intracellular accumulation compared to G4.5-Ce6-PEG (Fig. 3). These results are consistent with several reports demonstrating that the presence of PEG chains negatively affect the uptake of the nanoparticles *in vitro*.[33,34] Besides avoiding aggregation and preventing an opsonization during blood circulation, the PEG layer decreases the interactions
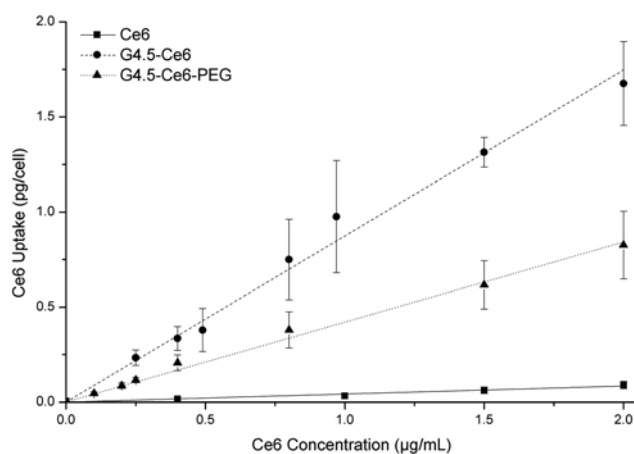

Fig. 3 Cellular uptake of free Ce6 (square), G4.5-Ce6 (round) and G4.5-Ce6-PEG (triangle) incubated with FaDu cells during 24 h as a function of the PS concentration.

2208 | *Photochem. Photobiol. Sci.*, 2015, **14**, 2203–2212

This journal is © The Royal Society of Chemistry and Owner Societies 2015

between the grafted chains and cell membrane leading to reduced cellular uptake,[33] a phenomenon known as the "PEG dilemma".[35] The enhanced uptake of G4.5-Ce6 and G4.5-Ce6-PEG (Fig. 3) could be responsible for better photocytotoxicity of dendrimer-based compounds (Fig. 2). However if the photo-toxicity is recalculated in terms of equivalent intracellular Ce6 concentration, it appears that the phototoxicity of NPs is 3 times less efficient compared to free Ce6. A major part of this difference can be explained by the lower singlet oxygen quantum yield of the PAMAM G4.5-modified Ce6 (Table 1). Moreover, subcellular localization could be of importance too.

Subcellular localization

The effect of vectorization on the subcellular distribution of Ce6 was investigated by CLSM with specific organelle fluorescent probes. Co-staining of FaDu cells with Lysotracker shows that Ce6 once associated with dendrimers was strongly localized in the lysosomes, with a Pearson's correlation coefficient >0.7 (Fig. 4 and 5). In contrast, free Ce6 was not found in the lysosomes (PCC < 0.35) but distributed elsewhere in the cell. Co-staining of Ce6-based compound mitochondria, Golgi apparatus and the ER was performed with Mitotracker, NBD and DioC6 respectively (Fig. 5 and S2†). All compounds had fairly the same localization pattern in these organelles, except

Fig. 4 CLSM images of lysosomal localization of Ce6, G4.5-Ce6 and G4.5-Ce6-PEG in FaDu cells. Left column displays confocal overlay images. These micrographs are representative of those obtained from three independent experiments. Right column shows the mean Pearson's correlation diagram. Red color corresponds to Ce6 and green color corresponds to LysoTraker® Green. Bar = 10 μm.

G4.5-Ce6 which is strongly confined to the Golgi apparatus while G4.5-Ce6-PEG and Ce6 were localized moderately in this organelle. As compared to ER or mitochondria, which are key organelles in the apoptotic cell death pathway, the PS localization in lysosomes is less favorable in terms of photocytotoxicity.[36,37] Thus, the next challenge could be the release of Ce6 from the dendrimer-based NP, paving the way to a further improvement of photoefficiency.

Internalization pathway and intracellular fate of the nanoconstructs

Fig. 6 displays an uptake inhibition carried out by incubation of NPs with cells under different conditions. At 4 °C, the internalization of Ce6 was unaffected, whereas the uptake of the two Ce6-dendrimers was lowered to 45% and 18% for G4.5-Ce6 and G4.5-Ce6-PEG, respectively. As energy-dependent cellular processes are inhibited at low temperature, we state that the free Ce6 internalization occurs via passive diffusion through the plasma membrane, as has already been demonstrated in many studies.[38–41] Contrarily, the dendrimer NPs mainly enter the cells via an active transport process. The fluorescence signal of Ce6 dendrimers observable at 4 °C could be attributed to diffusion or physical adhesion on the plasma membrane. This hypothesis is strengthened by the weaker internalization of PEGylated compared to non-PEGylated Ce6-dendrimers, most probably due to the well-known antifouling properties of the PEG layer.[42]

We further assessed the energy dependent internalization pathways as micropinocytosis, clathrin and caveolae uptake, using EIPA, chlorpromazine and genistein respectively (Fig. 6). We did not observe any uptake inhibition of Ce6-dendrimers after EIPA treatment. Therefore, the macropinocytosis is not a major cell uptake mechanism for the Ce6-dendrimers NP as recently claimed by Yuan *et al.*[43] Clathrin-mediated endocytosis (CME) pathway is inherent solely to G4.5-Ce6, while PEGylated dendrimers were indifferent to chlorpromazine-mediated inhibition ($p > 0.05$). As reported by Shcharbin *et al.* with identical PAMAM dendrimers,[44] serum components will be adsorbed at the surface of the G4.5-Ce6 to form a so called biomolecular corona,[45] providing the receptor–ligand recognition, necessary for CME.

On the other hand, the presence of the PEG layer leads to a strong decrease of serum protein adsorption as demonstrated elsewhere,[46,47] and as such G4.5-Ce6-PEG dendrimers are insensitive to the CME inhibition agent. Caveolae pathway endocytosis was assessed with genistein-mediated inhibition of Ce6 cellular uptake. Among both tested dendrimers, only uptake of the negatively charged G4.5-Ce6-PEG was mediated by the caveolae receptor-independent endocytosis pathway. Consistent with our study, it has been reported that negatively charged COOH terminated PAMAM G3.5 dendrimers were endocytosed via the caveolae pathway.[48]

Considering that G4.5-Ce6 and G4.5-Ce6-PEG display similar subcellular distribution patterns in the studied organelles, except that for the Golgi apparatus (Fig. 5), these results indicate that although the internalization mechanisms and
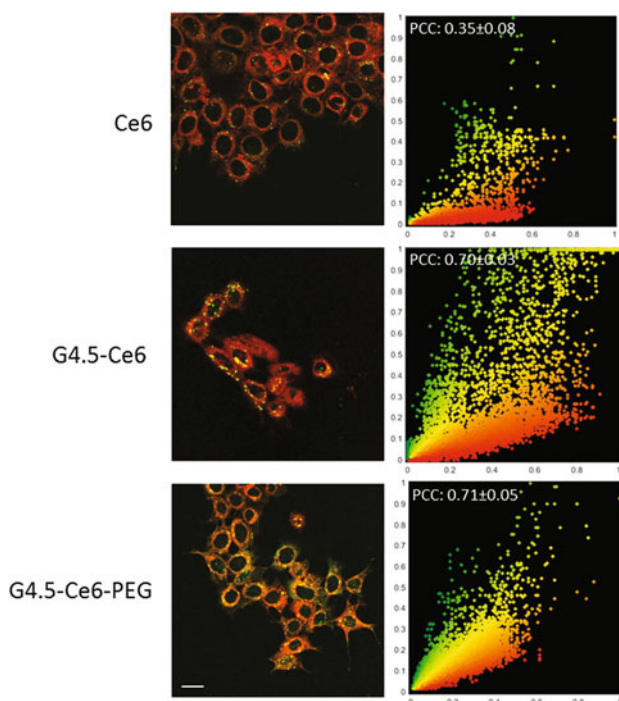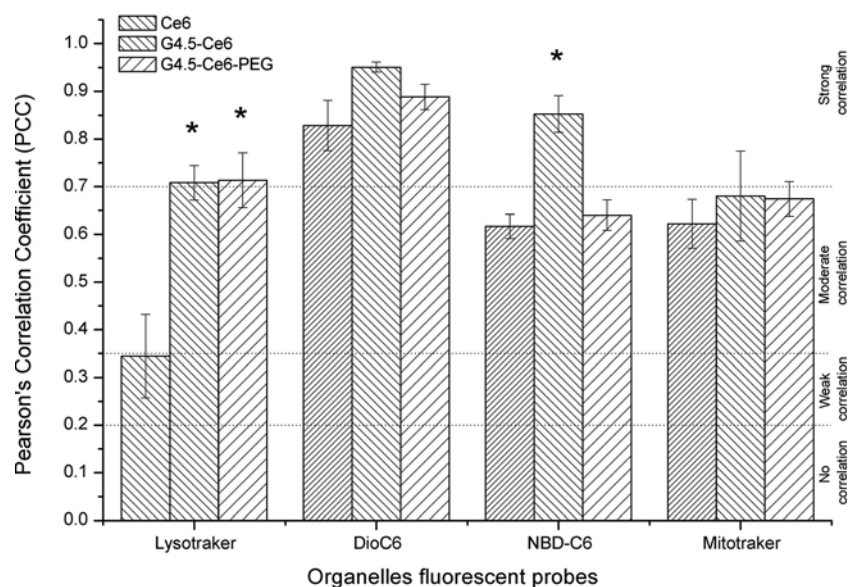
This journal is © The Royal Society of Chemistry and Owner Societies 2015

Photochem. Photobiol. Sci., 2015, **14**, 2203–2212 | **2209**

Fig. 5 Pearson's correlation coefficient (PCC) values quantifying the co-localization of the organelle fluorescent marker and free Ce6, G4.5-Ce6 or G4.5-Ce6-PEG in FaDu cells 24 h after incubation. PCC values of 1–0.7 indicate a relatively strong correlation, 0.69–0.36 indicate a moderate correlation, 0.35–0.2 indicate a weak correlation, and <0.2 indicates the absence of a correlation[26,27] (*$p < 0.05$ versus the free Ce6 group).
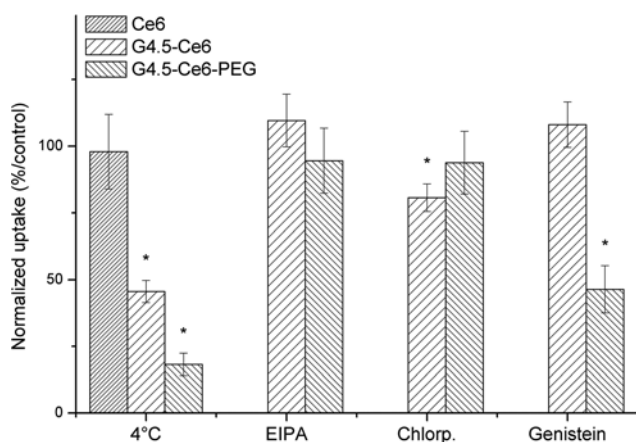

Fig. 6 Effect of various endocytosis inhibitors on cellular uptake of the PSs. FaDu cells were pre-incubated for 30 min at 4 °C without the endocytosis inhibitors or at 37 °C with inhibitors. After pre-incubation, PSs (final concentration 0.5 μg ml^{-1}) were added and incubated for 60 min, either in the presence of the inhibitors or at 4 °C (*$p < 0.05$ versus the untreated control group).

uptake of Ce6-dendrimers were different, the presence of PEG had little impact on the intra-cellular fate of the corresponding dendrimer. Moreover, despite the different incorporation mechanisms between Ce6 and Ce6-dendrimer, we observed a linear uptake in the function of PS concentration (Fig. 2). Considering the endocytosis NP-mediated pathway, compared to diffusion transport for free Ce6, we expected the saturation of dendrimers uptake. In all probability, the plateau could not be reached in the range of the tested concentrations

(0–2 μg mL^{-1}), while for higher concentrations a saturation of the uptake will definitely take place. Similar observations were reported earlier for gold nanoparticles.[49]

Besides that, we have been interested in the Ce6 and Ce6-dendrimers uptake measured as a function of incubation time (see figure below). We could observe the plateau in NPs uptake but not for free Ce6. This shows that the incorporation of our NPs can be saturated.

Classically, molecules that are internalized by the clathrin pathway are known to be subjected to lysosomal degradation[50] as opposed to the caveolae route which can avoid degradation.[51] However it has been shown in epithelial derived tumor cells that the caveolae and clathrin-mediated endocytosis pathways are connected and ends up in lysosomes.[52] Since FaDu cells belong to this category, it seems consistent that a certain proportion of the G4.5-Ce6-PEG is located in lysosomes.

Fluorescence lifetime imaging

Fluorescence lifetime imaging data are presented in Fig. 7. FaDu cells were incubated for 24 h with either free Ce6 or G4.5-Ce6 NPs. FLIM is a valuable technique to study the fluorophore properties in their microenvironment, such as photobleaching,[53] aggregation state[54] as well as their release from a NP.[55] Fluorescence lifetimes (τ) were measured before and after cell irradiation with a light dose of 3 J cm^{-2}. Before irradiation, τ values measured for G4.5-Ce6 and G4.5-Ce6-PEG were 5.1 ns and 4.9 ns, respectively, whereas it was significantly longer for free Ce6 (5.8 ns). After irradiation, the lifetimes of G4.5-Ce6 NPs remain unchanged, while τ drops to 4.3 ns for free Ce6. Upon light irradiation, we observed a decrease of the fluorescence intensity for free Ce6, accompanied by a
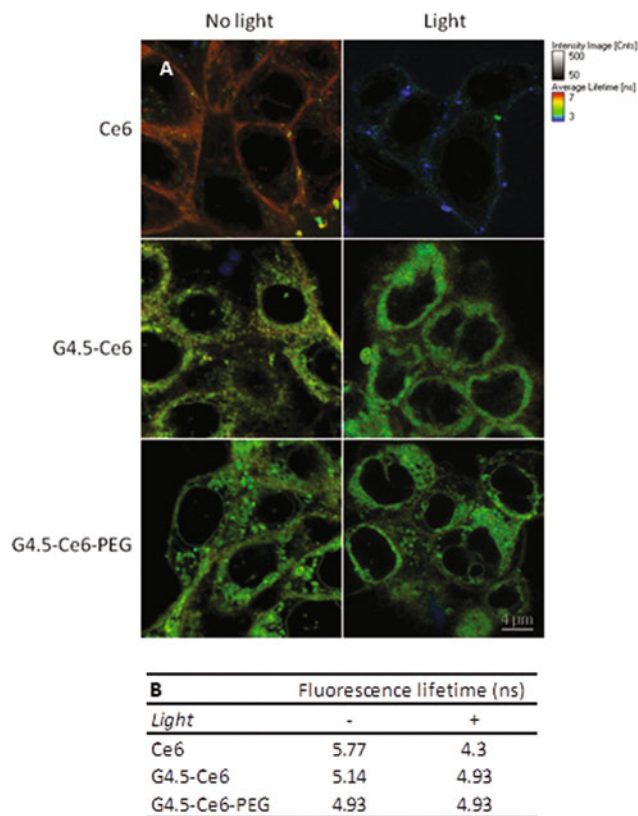
Fig. 7 Representation of fluorescence lifetime imaging microscopy (FLIM). FaDu cells were treated with 3 μM of free Ce6, G4.5-Ce6 or G4.5-Ce6-PEG. After 24 h, the cells were observed under a fluorescence-lifetime imaging microscope before and after irradiation (A). Average fluorescence lifetimes for each PSs were determined (B).

shortening of τ (Fig. 7). These changes for free Ce6, may be due to bleaching, relocalization or interaction with the local environment. However, no significant fluorescence lifetime changes were observed for G4.5-Ce6 and G4.5-Ce6-PEG, pointing out that Ce6 is not released from the dendrimer following irradiation.

Conclusion

PAMAM-Ce6 conjugates show a much higher photodynamic effect due to considerable internalization in the tumor cell model compared to free Ce6. Free Ce6 was shown to enter the cells by a simple diffusion mechanism, while G4.5-Ce6 and G4.5-Ce6-PEG internalization was dependent of active endocytosis pathway. However, the nanoparticles behave similarly in the cells since their subcellular localization was comparable. As a result, PEGylated G4.5 PAMAM-Ce6 dendrimers may offer an effective furtive biocompatible nanoparticle for photodynamic treatment in a preclinical tumor model. However, the reduced singlet oxygen quantum yield and pronounced localization in lysosomes indicate that great improvement of the photoefficiency of such nanoparticles is possible, if a release

of the PS from the dendrimers after cellular uptake can be realized.

References

1 N. Kuznetsova, N. Gretsova, V. Derkacheva, O. Kaliya and E. Lukyanets, *J. Porphyrins Phthalocyanines*, 2003, **7**, 147–154.

2 T. Trindade, P. O'Brien and N. Pickett, *Chem. Mater.*, 2001, **13**, 3843–3858.

3 V. Torchilin, *Adv. Drug Delivery Rev.*, 2011, **63**, 131–135.

4 N. Jux and B. Röder, in *Handbook of Porphyrin Science*, ed. K. Kadish, K. Smith and R. Guilard, World Scientific Publishing Co. Pte. Ltd., Singapore, 2010, vol. 4, pp. 327–401.

5 H. P. Lassalle, D. Dumas, S. Grafe, M. A. D'Hallewin, F. Guillemin and L. Bezdetnaya, *J. Controlled Release*, 2009, **134**, 118–124.

6 A. S. Derycke and P. A. de Witte, *Adv. Drug Delivery Rev.*, 2004, **56**, 17–30.

7 A. Preuss, S. Hackbarth, M. Wacker, T. Knobloch, K. Langer and B. Roder, *J. Controlled Release*, 2010, **148**, e117–e118.

8 S. Battah, S. Balaratnam, A. Casas, S. O'Neill, C. Edwards, A. Batlle, P. Dobbin and A. J. MacRobert, *Mol. Cancer. Ther.*, 2007, **6**, 876–885.

9 C. V. Synatschke, T. Nomoto, H. Cabral, M. Fortsch, K. Toh, Y. Matsumoto, K. Miyazaki, A. Hanisch, F. H. Schacher, A. Kishimura, N. Nishiyama, A. H. Muller and K. Kataoka, *ACS Nano*, 2014, **8**, 1161–1172.

10 M. Guo, H. Mao, Y. Li, A. Zhu, H. He, H. Yang, Y. Wang, X. Tian, C. Ge, Q. Peng, X. Wang, X. Yang, X. Chen, G. Liu and H. Chen, *Biomaterials*, 2014, **35**, 4656–4666.

11 M. Gary-Bobo, O. Hocine, D. Brevet, M. Maynadier, L. Raehm, S. Richeter, V. Charasson, B. Loock, A. Morere, P. Maillard, M. Garcia and J. O. Durand, *Int. J. Pharm.*, 2012, **423**, 509–515.

12 S. Hackbarth, V. Horneffer, A. Wiehe, F. Hillenkamp and B. Röder, *Chem. Phys.*, 2001, **269**, 339–346.

13 C. C. Lee, J. A. MacKay, J. M. Frechet and F. C. Szoka, *Nat. Biotechnol.*, 2005, **23**, 1517–1526.

14 L. M. Kaminskas, B. J. Boyd and C. J. Porter, *Nanomedicine*, 2011, **6**, 1063–1084.

15 E. R. Gillies and J. M. Frechet, *Drug Discovery Today*, 2005, **10**, 35–43.

16 N. Nishiyama, H. R. Stapert, G. D. Zhang, D. Takasu, D. L. Jiang, T. Nagano, T. Aida and K. Kataoka, *Bioconjugate Chem.*, 2003, **14**, 58–66.

17 N. Nishiyama, Y. Nakagishi, Y. Morimoto, P. S. Lai, K. Miyazaki, K. Urano, S. Horie, M. Kumagai, S. Fukushima, Y. Cheng, W. D. Jang, M. Kikuchi and K. Kataoka, *J. Controlled Release*, 2009, **133**, 245–251.

18 C. Kojima, Y. Toi, A. Harada and K. Kono, *Bioconjugate Chem.*, 2007, **18**, 663–670.

19 A. Francois, S. Battah, A. J. MacRobert, L. Bezdetnaya, F. Guillemin and M. A. D'Hallewin, *BJU Int.*, 2012, **110**, E1155–E1162.

20 E. Yeow, K. Ghiggino, J. Reek, M. Crossley, A. Bosman, A. Schenning and E. Meijer, *J. Phys. Chem. B*, 2000, **104**, 2596–2606.

21 M. Trester-Zedlitz, K. Kamada, S. K. Burley, D. Fenyo, B. T. Chait and T. W. Muir, *J. Am. Chem. Soc.*, 2003, **125**, 2416–2425.

22 J. A. Hargus, F. R. Fronczek, M. G. Vicente and K. M. Smith, *Photochem. Photobiol.*, 2007, **83**, 1006–1015.

23 D. M. Sweet, R. B. Kolhatkar, A. Ray, P. Swaan and H. Ghandehari, *J. Controlled Release*, 2009, **138**, 78–85.

24 S. Hackbarth, J. Schlothauer, A. Preuss and B. Röder, *Laser Phys. Lett.*, 2013, **10**, 125702.

25 F. Wilkinson, W. P. Helman and A. B. Ross, *J. Phys. Chem. Ref. Data*, 1993, **22**, 113–262.

26 R. G. Malgady and D. B. Krebs, *Phys. Ther.*, 1986, **66**, 110–120.

27 R. Taylor, *J. Diagn. Med. Sonogr.*, 1990, **6**, 35–39.

28 J. Megow, M. I. Rohr, M. Schmidt am Busch, T. Renger, R. Mitric, S. Kirstein, J. P. Rabe and V. May, *Phys. Chem. Chem. Phys.*, 2015, **17**, 6741–6747.

29 A. Kay, R. Humphry-Baker and M. Grätzel, *J. Phys. Chem.*, 1994, **98**, 952–959.

30 P. Li, G. Zhou, X. Zhu, G. Li, P. Yan, L. Shen, Q. Xu and M. R. Hamblin, *Photodiagn. Photodyn. Ther.*, 2012, **9**, 76–82.

31 H. Park and K. Na, *Biomaterials*, 2013, **34**, 6992–7000.

32 G. D. Zhang, A. Harada, N. Nishiyama, D. L. Jiang, H. Koyama, T. Aida and K. Kataoka, *J. Controlled Release*, 2003, **93**, 141–150.

33 E. C. Cho, Q. Zhang and Y. Xia, *Nat. Nanotechnol.*, 2011, **6**, 385–391.

34 Y. Li, M. Kroger and W. K. Liu, *Biomaterials*, 2014, **35**, 8467–8478.

35 H. Hatakeyama, H. Akita and H. Harashima, *Adv. Drug Delivery Rev.*, 2011, **63**, 152–160.

36 D. Kessel and Y. Luo, *J. Photochem. Photobiol., B*, 1998, **42**, 89–95.

37 M. H. Teiten, L. Bezdetnaya, P. Morliere, R. Santus and F. Guillemin, *Br. J. Cancer*, 2003, **88**, 146–152.

38 H. Mojzisova, S. Bonneau, C. Vever-Bizet and D. Brault, *Biochim. Biophys. Acta*, 2007, **1768**, 2748–2756.

39 U. Schmidt-Erfurth, H. Diddens, R. Birngruber and T. Hasan, *Br. J. Cancer*, 1997, **75**, 54–61.

40 N. S. Soukos, M. R. Hamblin and T. Hasan, *Photochem. Photobiol.*, 1997, **65**, 723–729.

41 J. D. Spikes, *J. Photochem. Photobiol., B*, 1990, **6**, 259–274.

42 K. Feldman, G. Hahner, N. Spencer, P. Harder and M. Grunze, *J. Am. Chem. Soc.*, 1999, **121**, 10134–10141.

43 A. Yuan, B. Yang, J. Wu, Y. Hu and X. Ming, *Acta Biomater.*, 2015, **21**, 63–73.

44 D. Shcharbin, J. Mazurb, M. Szwedzka, M. Wasiak, B. Palecz, M. Przybyszewska, M. Zaborski and M. Bryszewskaa, *Colloids Surf., B*, 2007, **58**, 286–289.

45 M. Lundqvist, J. Stigler, G. Elia, I. Lynch, T. Cedervall and K. A. Dawson, *Proc. Natl. Acad. Sci. U. S. A.*, 2008, **105**, 14265–14270.

46 J. L. Perry, K. G. Reuter, M. P. Kai, K. P. Herlihy, S. W. Jones, J. C. Luft, M. Napier, J. E. Bear and J. M. DeSimone, *Nano Lett.*, 2012, **12**, 5304–5310.

47 C. D. Walkey, J. B. Olsen, H. Guo, A. Emili and W. C. Chan, *J. Am. Chem. Soc.*, 2011, **134**, 2139–2147.

48 O. P. Perumal, R. Inapagolla, S. Kannan and R. M. Kannan, *Biomaterials*, 2008, **29**, 3469–3476.

49 J. D. Trono, K. Mizuno, N. Yusa, T. Matsukawa, K. Yokoyama and M. Uesaka, *J. Radiat. Res.*, 2011, **52**, 103–109.

50 F. R. Maxfield and T. E. McGraw, *Nat. Rev. Mol. Cell. Biol.*, 2004, **5**, 121–132.

51 R. G. Parton and K. Simons, *Nat. Rev. Mol. Cell. Biol.*, 2007, **8**, 185–194.

52 G. Sahay, J. O. Kim, A. V. Kabanov and T. K. Bronich, *Biomaterials*, 2010, **31**, 923–933.

53 M. Kress, T. Meier, R. Steiner, F. Dolp, R. Erdmann, U. Ortmann and A. Ruck, *J. Biomed. Opt.*, 2003, **8**, 26–32.

54 H. P. Lassalle, M. Wagner, L. Bezdetnaya, F. Guillemin and H. Schneckenburger, *J. Photochem. Photobiol., B*, 2008, **92**, 47–53.

55 Y. Li, H. T. Duong, S. Laurent, A. MacMillan, R. M. Whan, L. V. Elst, R. N. Muller, J. Hu, A. Lowe, C. Boyer and T. P. Davis, *Adv. Healthcare Mater.*, 2015, **4**, 148–156.